Dislocation Injection, Reconstruction, and Atomic Transport on {001} Au Terraces

Henny W. Zandbergen,[1,2] Chun-Wei Pao,[2] and David J. Srolovitz[2,3]

[1]*National Centre for HREM, Kavli Centre of Nanoscience, Delft University of Technology, 2628 CJ Delft, The Netherlands*
[2]*Princeton Institute for the Science and Technology of Materials, Princeton University, Princeton, New Jersey 08544, USA*
[3]*Department of Physics, Yeshiva University, New York, New York 10033, USA*

(Received 14 February 2006; published 18 January 2007)

High-resolution electron microscopy investigations of Au films show that adatoms on (100) surfaces insert into the underlying terrace to form surface dislocations. This injection readily occurs when the number of adatoms on a terrace is ~20 atoms or less. The surface dislocation glides along the terrace, but is repelled from the edges. The dislocation escapes by squeezing out in the dislocation line direction (not gliding out the terrace edge). Atomistic simulations confirm the dislocation stability, easy glide along the terrace and trapping at the terrace edge. These results have profound implications for film growth.

DOI: 10.1103/PhysRevLett.98.036103 PACS numbers: 68.35.Bs, 68.37.Lp

The growth and/or evaporation of a film are complex dynamical processes. To exercise control over film uniformity and surface morphology requires a high level of understanding of the detailed atomistic mechanisms of surface processes during growth and evaporation. Such processes include surface transport mechanisms, such as atomic hopping along the surface [1], atomic exchanges between surface adatoms and atoms within a terrace or at a step [1,2], diffusion across or over a step [3], and diffusion into or out of grain boundaries [4]. For example, energy barriers (Ehrlich-Schwöbel barrier [5]) associated with atoms hopping down surface steps (from an upper terrace to a lower one), can lead to three-dimensional growth [6].

Surface reconstructions can play an important role in growth processes. Reconstructions that occur during growth may or may not be the same as in equilibrium. Still, they give an indication of the tendencies of the surface for structural change and, as such, can aid in the understanding of growth surfaces. Au {100} surfaces reconstruct into a quasihexagonal structure leading to a (5×1) superperiodicity [7,8], resulting in a 20% increase in the atom density. {110} and {111} Au surfaces adopt a (1×2) reconstruction, yielding narrow {111} microfacets [9,10] and a $(\sqrt{3} \times 22)$ reconstruction consisting of a lateral compression along ⟨110⟩ by 4.4%, respectively. While such surface reconstructions occur in high vacuum [11,12] and in an electrolyte [13], they can be disturbed by gas adsorption [11], application of an electrical field [12] or by changing electrolytes [13]. For example, depositing adatoms on unreconstructed Pt(111) leads to the reconstruction of this surface, characterized by a fairly regular surface dislocation network [14]. Simulations in which adatoms are placed in a restricted region of the surface have shown that these can indeed produce a surface dislocation loop [15]. In this Letter, we report high-resolution electron microscopy (HREM) and atomistic simulation results that show the surface dislocation injection process, and how surface dislocations move and annihilate on a (unreconstructed) (001) gold surface. These surface dislocations are not simply surface structural features but are highly mobile, dynamic defects. These dynamical changes affect adatom incorporation, provide a surface transport mechanism, and are related to the equilibrium reconstruction. Such processes shed new light into the interplay of surface reconstuction and surface stress.

Gold films were prepared by evaporation onto a (110) cleaved NaCl substrate at 300 C. The 20 nm thick films consisted of single crystalline areas in [110] orientation. The NaCl was dissolved in water and the floating Au film was captured on a Au grid. High-resolution electron microscopy was performed with a Philips CM-300 UT-FEG TEM at an accelerating voltage of 300 kV. Spot sizes between 100 and 400 nm were used with a current of ~5 nA (i.e., $\sim 10^6$ electrons/s nm^2). The edges of the thin Au film tend to be rounded and were sculpted using the electron beam (to displace atoms which then move by surface diffusion and/or evaporate) into hillock structures such as that shown in Fig. 1(a). The hillock surface exposes a series of {001} terraces and the electron beam is oriented along [110]. Figure 1(b) shows the hillock in three geometries. In Fig. 1(b) (top) the hillock is seen from "above" (viewed in the [001] direction), which is the view that would be obtained using scanning probe microscopy (SPM) imaging. SPM observations would accurately show the positions of the surface atoms both laterally and normal to the surface, but would provide no information on the underlying atoms and the registry of the surface atoms relative to these. Figure 1(b) (middle) shows a side view of the hillock along [110] atom columns, as viewed in the HREM experiments reported herein. Since transmitted electrons in HREM are used, one "sees" atom columns, rather than individual atoms. The lateral atom column positions are accurate, but the positions of the atoms in the direction along the column is absent. Figure 1(b) bottom shows a geometry tilted away from the [110] orientation to show the relation between the two upper geometries. The following notation is adopted: the atomic plane containing relatively few atoms on the top of the hillock is denoted as plane A (red circles in Fig. 1), the next atomic plane as plane B (blue circles in Fig. 1), etc. The

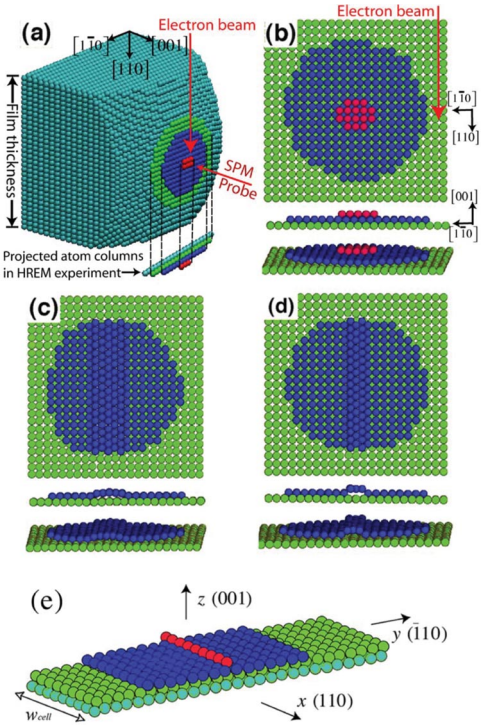

FIG. 1 (color online). (a) Schematic illustration of the HREM experiment, indicating the orientation of the surface and surface terraces relative to the electron beam and how they are seen in the HREM image. (b) The atoms in a cluster on plane A atop the plane B terrace. Three representations of the atomic configurations of the adatoms from plane A in three different viewing directions (the middle one is the [110] TEM viewing direction). (c) The adatoms injected from plane A into plane B to form a type 1 dislocation and (d) into plane B to form a type 2 dislocation. Note that the dislocation core consists of a hexagonal arrangement of Au atoms and that the width of this hexagonal stripe is two atom columns wider for type 1 than type 2. (e) Schematic illustration of the atomistic simulation cell geometry.

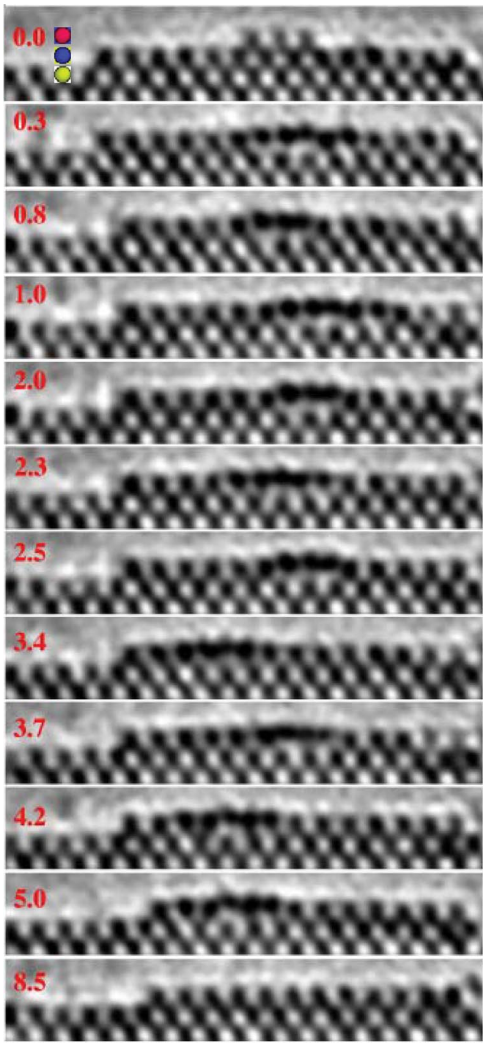

FIG. 2 (color online). Series of HREM images taken from a movie [16]. The black dots represent Au atom columns along the viewing direction (i.e., [110]). The time is indicated on the left in seconds. In the top image red, blue and green dots show the correspondence of the atom planes (A, B, and C) to the schematic in Fig. 1. In the middle ten figures a dislocation can be observed in the top atom layer (plane B). Between 5.0 s and the movie frame immediately prior to the 8.5 s image (not shown), the dislocation does not move. The contrast in these images was enhanced by applying Fourier filtering (reducing the contrast of features larger than 0.8 nm and smaller than 0.06 nm). Note, that the 8.5 s configuration is very similar to that at 0 s, except that at 0 s some adatoms are present on top of the terrace. If some of the atoms are removed from the flat terrace after 8.5 s or additional adatoms are put onto the flat terrace, the 0 s configuration is recreated and the whole process repeats.

specimen holder was at ~40 °C during the HREM experiments. Although the electron beam can produce some local heating, this should not increase the temperature of the sample by more than 10 °C. It is possible, however, for the electron beam to knock an atom from its position. The system typically "repairs" this quickly, but the breaking and reestablishment of these bonds can lead to a very localized (in time and space) temperature spike. In this sense, the macroscopic concept of temperature is not completely applicable during a HREM experiment.

Figure 2 shows a sequence of HREM images of an evolving (001) surface selected from a movie [16]. At 0 sec there are still Au atoms in plane A. The black dots are atom column positions along the viewing direction and consist of 3–4 atoms (as deduced from detailed analysis of the contrast). In order to minimize the length of the step surrounding the terrace, the terrace shape is expected to be compact (nearly circular). Note that the observed (001) surface layer is bulklike rather than the 5×1 reconstruction found on well-equilibrated, large, clean surfaces. At 0.1 sec the atoms that were in plane A are injected into plane B resulting in the formation of an extra row of Au atoms. This extra row of atoms can be thought of as a string of interstitials in the surface plane or as an edge dislocation lying in the surface plane along the [110] direction with a $(a_0/2)[1\bar{1}0]$ Burgers vector. This dislocation is quite mobile, gliding along the plane B terrace (see Fig. 2).

Although mobile, the dislocation appears unable to escape through the edge of the terrace (i.e., the step), but rather remains trapped in plane B for 10 seconds. In other cases, this trapping was observed to last several minutes. The dislocation is also observed to reside for long periods of time near the center of the terrace (0.8 sec) or near one of the terrace edges (3.4, 4.2, and 5.0 sec images). This preference for a position close to the edges is typical for surface terraces that are 10 to 20 atoms wide. In wider ones, the dislocation tends to stay in the middle of the terrace. Note, the number of atom columns in plane B is reduced by one in between the 0.3 and 0.8 s images and between the 4.2 and 5.0 s images, presumably due to fast diffusion along the step edge and onto the (110) film surface. The formation of surface edge dislocations was observed in approximately 75% of all cases that plane A was removed.

Two rather stable atom configurations of the surface dislocation are observed: these are typified by the one at 0.3 sec (type 1) and the other at 0.8 sec (type 2). Models for the atomic arrangements of type 1 and type 2 are shown in Figs. 1(b) and 1(c), respectively. Type 1 is observed very frequently close to the plane B edge (at 3.4, 4.2, and 5.0 sec). In fact, type 1 dislocations are quite stable near the edges (where they appear to be trapped) but may move rapidly from being trapped at one edge of plane B to being trapped at the opposite side of plane B. Type 2 dislocations are only observed near the center part of plane B.

In almost all cases, the escape of the surface dislocation does not lead to the widening of the terrace by one extra atom column or appearance of adatoms on top of plane B. This indicates that the atom column at the core of the dislocation is squeezed out of plane B along the electron beam direction. This process is very fast and was not observed in the 0.05 sec interval between frames of the movies. The atoms that are squeezed out probably end up on the back or front side of the island, incorporated into the next terrace down (plane C) or on the (110) surface of the film. The HREM observations do not allow us to distinguish between these.

In order to understand the formation and motion of the observed surface dislocations, we performed a series of atomistic (conjugate gradient minimization and molecular dynamics) simulations using a modified embedded atom method potential for Au [17]. A schematic illustration of the simulation cell employed to determine surface dislocation energetics is shown in Fig. 1(e) [the (001) surface has the bulk termination, as observed experimentally—Fig. 2]. The formation energy of a surface dislocation (per unit length) $E_f(y)$, parallel to the x axis, is

$$E_f(y) = [E_d(y) - E_{\text{ref}}]/w_{\text{cell}}, \quad (1)$$

where y labels the position of the dislocation, $E_d(y)$ is the energy of the system containing the surface dislocation centered at y in plane B and relaxed at 0 K, E_{ref} is the energy of the reference system with the column of atoms in plane A [as per Fig. 1(e)] and w_{cell} is the simulation cell width (in the x direction).

If the column of adatoms in plane A [Fig. 1(d)] is pushed into plane B at 0 K, it spontaneously relaxes back to the column of adatoms configuration; no surface dislocation is formed. On the other hand, if this configuration is heated to 900 K for 10 ps and then cooled to 300 K over 20 ps the type 2 surface dislocation, as shown in Fig. 1(c), is obtained. If the surface dislocation shown in Fig. 1(b) (type 1) is created and relaxed at 300 K for 1 ns, it is also found to be stable. These results show that the two types of surface dislocations do not form spontaneously at low temperature during the course of our short molecular dynamics simulations, but are at least metastable. The formation energies E_f of both the type 1 and 2 surface dislocations are shown in Fig. 3 as a function of y/L_0 is shown in Fig. 3 for terraces (plane B) of different lengths L_0 (in the y direction). The simulations show that for all surface dislocation positions y, the surface dislocation has lower energy than the row of adatoms (i.e., $E_f < 0$). Since the energy of the system rises rapidly as the type 1 or type 2 surface dislocations approach the terrace edge, the surface dislocations are unable to escape the terrace by crossing the step. Figure 3 also demonstrates that the type 1 surface dislocation is stable with respect to the type 2 surface dislocation (and the column of adatoms configuration). Both type 1 and type 2 dislocation were observed in our experiments (e.g., see Fig. 2 at $t = 2.3$ and 2.0 s, respectively), with the type 1 structure being the most common. Hence, the simulation results and experimental observations are consistent.

The formation energy vs y plot (Fig. 3) also shows that except near the terrace edges, the surface dislocation energy is nearly independent of position along the terrace (away from the edges, the energy landscape is rather flat). However, careful examination of the data demonstrates that the minimum energy configuration for type 1 disloca-

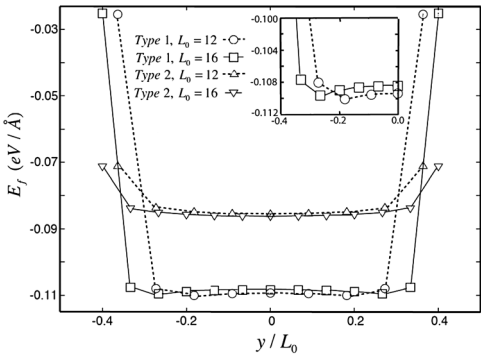

FIG. 3. The formation energy of the surface dislocations E_f of types 1 and 2 versus dislocation position y for terraces of several lengths L_0. The zero of the horizontal axis corresponds to the middle of the terrace. Since the dislocation is unstable at the two ends of the terrace, the first and last data points in the figure do not occur at $\pm 0.5L/L_0$. The inset shows the same data for the type 1 dislocation at a higher resolution. Note that the numerical errors are much smaller than the data points in the figure.

tions corresponds to the dislocation near the terrace edge (see the inset in Fig. 3). The type I surface dislocation is, however, unable to escape from the terrace because of the rapid rise in energy immediately at the terrace edge. The minimum energy configuration for the type 2 surface dislocation occurs at the center of the terrace. These predictions are also consistent with the experimental observations. That is, the type 1 dislocation is observed in experiment to move towards the terrace edge and become trapped there, while type 2 dislocations are never observed adjacent to the terrace edge. Both types of surface dislocations are repelled from the actual step; this repulsion is very short-ranged. This presumably results from the fact that the dislocation core is of finite extent and, hence, moving the dislocation up to the step requires dislocation core reconstruction. This also explains why the repulsion is stronger for type 1 dislocations than type 2 (note the rapid rise in E_f at the extrema of y/L_0 in Fig. 3); that is type 2 have narrower cores than do type 1 dislocations by two [110] atom columns.

The formation of the surface dislocations can be related to the equilibrium reconstruction of the (001) surface [7,8]. This reconstruction is (5×1) and corresponds to a regular array of parallel surface edge dislocations (of the type seen here) separated by five interatomic spacings. In contrast to this regular array on large, flat, clean surfaces, only a single (5×1) reconstruction stripe is observed in our experiments, although there is space for more of them. Nevertheless the atomic displacements in the stripe are reminiscent of the (5×1) structure. Therefore, the injection of the surface dislocations seen here is fundamentally the process of reconstruction. However, in a terrace of finite size and with a finite number of adatoms available, it is not always possible to create the requisite dislocation density. Further, the effect of the steps at the ends of the surface must also break the (5×1) periodicity. With a smaller than equilibrium density of surface dislocations, there is nothing to prevent the surface dislocation from migrating back and forth across the terrace, as seen here.

Why does the surface dislocation and equilibrium reconstruction form? The present results do not fully answer this question but do provide interesting hints. The surface stress on the unreconstructed surface is large and tensile. The presence of adatoms on the surface has little effect on this surface stress [18]. When adatoms collectively inject into the terrace and form a surface dislocation (of either type), the tensile surface stress is greatly reduced. Therefore, surface dislocation injection and the equilibrium reconstruction are likely driven by surface stress relaxation. Note that the presence of a step relaxes the stress within the terrace over a distance of order a few interatomic spacings. Therefore, the dislocation is not needed to relax the surface stress near the step and hence avoids the island edge. The same idea can be expressed in terms of the interaction of the elastic fields of the surface edge dislocation and the surface stress. This leads to a repulsive interaction in the present case. All of this is consistent with the dislocation being repelled from the edge of the terrace seen in the experiments and simulations.

Finally, it is interesting to note that the motion of the surface dislocation along the terrace is a very efficient means to transport atoms (in the direction perpendicular to the surface dislocation line direction). The experiments also show that the surface dislocation can escape the terrace. If we consider the process of the formation, translation, and escape of the surface dislocation (or a surface interstitial) altogether, we have a new picture for translating an atom from atop a terrace onto the next terrace down. There is a barrier for the direct hopping from one terrace to another (the Ehrlich-Schwoebel barrier [5]) that has profound consequences for film growth morphologies. The present mechanism of translating atoms from terrace to terrace provides an alternative pathway to achieve the same result. At this point, the relative magnitude of the barriers associated with the different pathways remains largely unexplored.

The authors thank useful discussion with Professors Carl Thompson and Daryl Chrzan. C. W. P. and D. J. S. gratefully acknowledge the support of the U. S. Department of Energy (Grant No. DE-FG02-99ER45797).

[1] G. Boisvert and L. J. Lewis, Phys. Rev. B **56**, 7643 (1997).
[2] G. L. Kellogg and P. J. Feibelman, Phys. Rev. Lett. **64**, 3143 (1990).
[3] W. Zhu, F. B. de Mongeot, U. Valbusa, E. G. Wang, and Z. Zhang, Phys. Rev. Lett. **92**, 106102 (2004).
[4] E. Chason, B. W. Sheldon, L. B. Freund, J. A. Floro, and S. J. Hearne, Phys. Rev. Lett. **88**, 156103 (2002).
[5] R. L. Schwoebel and E. J. Shipsey, J. Appl. Phys. **37**, 3682 (1966); G. Ehrlich and F. G. Hudda, J. Chem. Phys. **44**, 1039 (1966).
[6] J. Villain, J. Phys. I **1**, 19 (1991).
[7] D. G. Fedak and N. A Giostein, Surf. Sci. **8**, 77 (1967).
[8] M. A. Van Hove, R. J. Koestner, P. C. Stair, J. P. Biberian, L. L. Kesmodel, I. Bartos, and G. A. Somorjai, Surf. Sci. **103**, 189 (1981).
[9] W. Moritzand and D. Wolf, Surf. Sci. **163**, L655 (1985).
[10] I. Moller, H. Niehusand, and W. Heiland, Surf. Sci. **166**, Lll I (1986).
[11] M. P. Cox, G. Ertland, and R. Imbihl, Phys. Rev. Lett. **54**, 1725 (1985).
[12] J. Buisset, H. P. Rust, E. K. Schweizer, L. Cramer, and A. M. Bradshaw, J. Vac Sci. Technol. B **14**, 1117 (1996).
[13] A. S. Dakkouri, Solid State Ionics **94**, 99 (1997).
[14] M. Bott, M. Hohage, T. Michely, and G. Comsa, Phys. Rev. Lett. **70**, 1489 (1993).
[15] J. Jacobsen, K. W. Jacobsen, and P. Stoltze, Surf. Sci. **317**, 8 (1994).
[16] See EPAPS Document No. E-PRLTAO-98-052703 for a real-time HREM movie. For more information on EPAPS, see http://www.aip.org/pubservs/epaps.html.
[17] M. I. Baskes, Phys. Rev. B **46**, 2727 (1992).
[18] C. W. Pao, D. J. Srolovitz, and C. V. Thompson, Phys. Rev. B **74**, 155437 (2006).